Titre: Title:	Remote electric powering by germanium photovoltaic conversion of an erbium-fiber laser beam
Auteurs: Authors:	Richard Soref, Francesco De Leonardis, Oussama Moutanabbir, & Gérard Tanguy Eric Gnato Daligou
Date:	2024
Type:	Article de revue / Article
Référence: Citation:	Soref, R., De Leonardis, F., Moutanabbir, O., & Daligou, G. T. E. G. (2024). Remote electric powering by germanium photovoltaic conversion of an erbium-fiber laser beam. Chip, 3(3), 100099 (13 pages). https://doi.org/10.1016/j.chip.2024.100099

Document en libre accès dans PolyPublie
Open Access document in PolyPublie

URL de PolyPublie: PolyPublie URL:	https://publications.polymtl.ca/58725/
Version:	Version officielle de l'éditeur / Published version Révisé par les pairs / Refereed
Conditions d'utilisation: Terms of Use:	CC BY

Document publié chez l'éditeur officiel
Document issued by the official publisher

Titre de la revue: Journal Title:	Chip (vol. 3, no. 3)
Maison d'édition: Publisher:	Elsevier
URL officiel: Official URL:	https://doi.org/10.1016/j.chip.2024.100099
Mention légale: Legal notice:	© 2024 The Author(s). Published by Elsevier B.V. on behalf of Shanghai Jiao Tong University. This is an open access article under the CC BY license (http://creativecommons.org/licenses/by/4.0/).

Chip

Remote electric powering by germanium photovoltaic conversion of an Erbium-fiber laser beam

Richard Soref[1,*], Francesco De Leonardis[2] , Oussama Moutanabbir[3] & Gerard Daligou[3]

[1]Engineering Department, University of Massachusetts at Boston, Boston, MA 02125, USA [2]Department of Electrical and Information Engineering, Politecnico di Bari, Bari 70121-70132, Italy [3]Department of Engineering Physics, Ecole Polytechnique de Montreal, Montreal, Quebec 999040, Canada

*E-mails: richard.soref@umb.edu (Richard Soref)

The commercially available 4000-Watt continuous-wave (CW) Erbium-doped-fiber laser, emitting at the 1567-nm wavelength where the atmosphere has high transmission, provides an opportunity for harvesting electric power at remote "off the grid" locations using a multi-module photovoltaic (PV) "receiver" panel. This paper proposes a 32-element monocrystalline thick-layer Germanium PV panel for efficient harvesting of a collimated 1.13-m-diam beam. The 0.78-m² PV panel is constructed from commercial Ge wafers. For incident CW laser-beam power in the 4000 to 10,000 W range, our thermal, electrical, and infrared simulations predict 660 to 1510 Watts of electrical output at the panel temperatures of 350 to 423 K.

Keywords: Laser power transmission, Photovoltaic panels, Germanium infrared detection, Erbium fiber laser, Ytterbium fiber laser, Directed-beam energy harvesting

INTRODUCTION

In the emerging field of "power by light"[1,2], which is also known as laser power transmission (LPT)[3] and optical wireless power transfer[4–15], the experiments reported in the literature utilized a continuous-wave (CW) laser-beam output power of 50 Watts or less. This prior art does not include recent advances in the CW short-wave infrared (SWIR) laser art. The present paper targets lasers that emit in the SWIR defined here as the 900 to 1700-nm wavelength region. In addition, the present paper considers only the commercially available lasers whose CW output power is 4000 Watts or more, which are defined as ultra-high power (UHP) laser transmitters. A scan of the laser-development literature and a

survey of reports from laser manufacturers reveals that there exist currently only two UHP SWIR lasers. They are the Ytterbium-doped fiber laser (YFL) emitting at the 1075-nm center wavelength and the Erbium-doped fiber laser (EFL) emitting at the 1567-nm wavelength. The beams of both lasers travel with very low loss through the earth's atmosphere due to the atmosphere's transparency for those waves.

In this UHP context, a recent theoretical-physics paper by the present authors[16] predicted efficient optical-to-electrical (OE) conversion, or "harvesting" of the YFL beam by a multi-module silicon photovoltaic (PV) "panel"[16], to the best of our knowledge, this is the first UHP-beam-harvesting paper. The present paper is the second UHP-OE-conversion paper, and this present work is motivated by the fact that the silicon PV panel of[16] cannot and will not harvest the EFL beam because the 1.12 eV silicon bandgap energy is well above the 0.79 eV EFL photon energy. An alternative PV is needed, and an elemental semiconductor PV is the simplest and perhaps the best choice. In view of that, a new aspect of this paper is that we proposed an optimum semiconductor PV panel to harvest the EFL; specifically, we proposed and analyzed the mono-crystalline thick-layer Germanium PV panel to provide efficient and effective EFL OE conversion. This is a new Ge panel which hasn't been discussed in the literature. The literature instead reports thin-film and heterojunction Ge modules[17–24]. We show simulations of panels with modules fabricated from 300-mm commercial Ge wafers. Our numerical modeling includes large-area series-connected panels that harvest a collimated large-area EFL beam. An additional new aspect here is that we quantify the Ge PV panel's harvesting of the YFL, which is an added benefit of the Ge approach. The EFL mission is primary here, while the YFL harvesting is secondary but quite useful.

The sections of this paper include a background discussion, design of the encapsulated Ge PV-diode module, thermal-and-electrooptical simulations of this module, numerical results for the conversion efficiency of Ge+EFL and Ge+YFL, a comparison to Si+YFL conversion, the optimized 32-module Ge panel, Ge TPV, and the Ge+EFL system offering both radio-frequency (RF) communications and direct-current (DC) electric output.

BACKGROUND DISCUSSION

Since the EFL photon energy is above the 0.66 eV Ge bandgap, the Ge+EFL system offers efficient conversion and large electric output. Since several commercial vendors offer oriented crystal Ge wafers in

diameter up to 300 mm, this paper proposes the use of large-area 156 mm × 156 mm monocrystal Ge PV modules that are fabricated from those wafers. Those modules are then grouped into a planar Ge PV "panel", such as a 32-element array that gives good overlap with a large diameter of the collimated incident laser beam. It is an array in which the constituent modules are interconnected electrically in series. This panel is quite analogous to a Si solar panel in terms of its layout and its construction or "encapsulation". Another Ge-to-Si PV similarity is the utilization of "thick layers" in each Ge PN junction, specifically a Ge PN diode with the total thickness of 180 μm is used here. A motivation here is to reach kilowatt electric output using commercial EFLs. There is an EFL available at the 4,000 W CW level[25], and this output could in principle be increased to 10,000 W CW in a custom product.

Regarding system details, in order to obtain targeting, the EFL would be mounted in an aiming device (for example, mounted in a tilt/rotation turret on top of a truck) so that the beam can be directed to impinge upon the remotely located PV receiver. The laser can be ship-borne or space-borne or airborne or on-ground as described.

There are numerous remote-powering applications such as the 11 scenarios listed in ref.[16] (all of which apply here) where the PV-panel receiver is in an "off the grid" location, and where fuel-powered portable electric generators are not readily available or not desired. If the PV electricity is not immediately used, the LPT can be used to charge storage batteries.

It should be stated that at the outset that the Ge laser power system (and such systems generally) faces barriers to their widespread adoption. These challenges are in the areas of economics and safety. In particular, the system cost is high due to the capital cost of the UHP laser, and higher cost of Ge PV than that of Si PV. When considering the energy that must be supplied to actuate the laser, the overall energy efficiency (i.e., energy-in/energy-out) of the LPT might be low. There exist issues of eye safety in the transmitter and receiver, and for the case of 20 kW lasers, the high operation temperature of the PV panel might be hazardous. However, in some cases/applications, the advantages of LPT outweigh the disadvantages.

THERMAL AND ELECTRICAL-OPTICAL SIMULATIONS

Photovoltaic Module Design For the optical wireless system in ref.[16], we adopted the multi-material "encapsulation" architecture of the commercial monocrystal silicon solar cell for the Si PV module. Because of the success of that approach, we have decided to utilize the same multi-material construction for the LPT Ge PV module, as illustrated in Fig. 1.

In Fig. 1, if we define t as the "optimum" overall thickness of the mostly P- region plus N-region, there is a design rule for determining t, which is $t = 1/\alpha$, where α is the room-temperature absorption coefficient of the dominant P-type Ge at the 1567-nm wavelength. Turning to the Ioffe reference compilation[26], it is found that $\alpha = 55$ cm^{-1}, yielding $t = 180$ μm. This is a layer thickness that is generally much higher than that produced by Ge epitaxial growth procedures, which implies that Fig. 1 diode is simply fabricated from a P-type Ge commercial wafer.

Numerical Results A general theoretical approach to simulating the thermal and optical-electrical responses of the large-area PV module was presented in ref.[16], including six equations that quantified the PV performances. We have adopted the same modeling-and-simulating framework and equations for Ge, and have taken the necessary Ge experimental parameters according to the literature[26], such as the
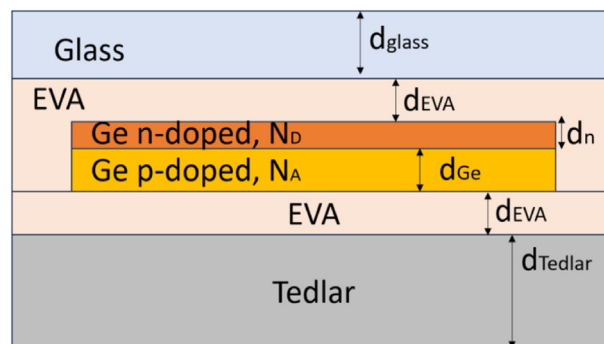

Fig. 1 | Cross-section view of Ge PV cell utilizing the commercial Si solar cell architecture. Relevant parameters and materials are indicated. The cell has an area of 15.6 cm × 15.6 cm. For the n-doped layer: $d_n = 0.2$ μm, $N_D = 10^{19}$ cm^{-3}. For p-doped layer: $d_{Ge} = 180$ μm, $N_A = 10^{17}$ cm^{-3}.

infrared absorption coefficients versus wavelength, and bandgap versus temperature[26]. The infrared absorption coefficient and the Ge bandgap narrowing effect[26] have been fitted by means of Eq. (18) of ref.[27] and Eq. (1) of ref.[28], respectively. Moreover, carrier mobilities and effective masses have been evaluated with the adoption of the diffusion co-efficients and the effective density states given in Table 1 and 2 of ref.[29]. With the adoption of this framework, we made a set of calculations whose results are given in Fig. 2−5 as follows.

These are the parameters used for simulating Fig. 1 thermal responses.

Here, it is assumed that a finned heat sink is in contact with the rear surface of the PV to provide passive cooling of the PV, that is, cooling by convection of ambient air.

Regarding the OE conversion efficiency calculated in Fig. 2 and 4, the Gaussian shape of the beam laser has been taken into account by applying Eq. (4) of ref.[16]; that is, for a laser beam having a Gaussian spatial distribution, the laser flux on the top PV surface is given by:

$$Flux = (1 - R)\frac{2 \cdot P_{laser}}{\pi \cdot r_{sp}^2}e^{\left(-2\frac{(x-x_{focus})^2+(y-y_{focus})^2}{r_{sp}^2}\right)}$$

where, R denotes the reflectivity at the top glass surface, P_{laser} is the laser power arriving at this PV surface and r_{sp} represents the laser spot radius (where the beam intensity has fallen down to $1/e^2$ of the central beam power). The terms x and y are the coordinates in the xy plane of the PV cell, x_{focus} and y_{focus} represent the center point of the spot. In turn, the laser Flux is used to characterize the heat source in each PV layer, according to the Beer-Lambert law, given by Eq. (2) of ref.[16]. In our simulations, it is assumed $r_{sp} = 80$ cm, and we have considered the effective area of the beam $A_b = \pi r_e^2$, where r_e is the

Table 1 | Physical Parameters of thermal simulations.

Parameters	Materials			
	Germanium	Glass	EVA	Tedlar
Density [kg/m³]	5323	2450	950	1200
Thermal conductivity [W/mK]	60	2	0.311	0.15
Heat capacity at constant pressure [J/kgK]	310	500	2090	1250

Table 2 | Summary of results.

PV and FL	CW laser power output [W]	Metrics			
		PV body temperature [K]	Efficiency [fractional]	Output electric power density [W/m²]	Output electric power [W] For A = 0.0243 m²
Ge+EFL 1567 nm	4000	350	0.27	1055	26
Ge+EFL 1567 nm	10,000	423	0.25	2412	59
Ge+EFL 1567 nm	20,000	518	0.21	4056	99
Ge+YFL 1075 nm	4000	354	0.18	680	17
Ge+YFL 1075 nm	10,000	427	0.16	1533	37
Ge+YFL 1075 nm	20,000	520	0.13	2550	62
Si+YFL 1075 nm	4000	320	0.13	530	13
Si+YFL 1075 nm	10,000	401	0.26	2546	62
Si+YFL 1075 nm	20,000	564	0.31	6272	152

effective beam-spot radius given by $r_e = r_{sp}/\sqrt{2}$, yielding $A_b = \pi r_{sp}^2/2$. Moreover, our investigations indicate that the maximum OE conversion efficiency decreases weakly with the increasing spot radius.

In Fig. 4, an initial rise in the maximum conversion efficiency is observed with increasing laser power, and subsequently there appears a decline in efficiency with further increase of laser. This behavior can be explained by taking into account of the "thermal aspects" as follows: under monochromatic illumination, the temperature dependence of the conversion efficiency induces the existence of T_{peak} to which corresponds a peak in the maximum conversion efficiency. The existence of this peak is induced by the complex temperature dependence given by Eqs. (2), (3) and (6) of ref.[16]. In the present system, as the PV

(a)

(b)

Fig. 3 | Calculated temperature distribution in a 156 mm × 156 mm germanium PV module. a, Laser power 4000 W and $d_{Ge} = 180$ μm. **b,** Laser power 10,000 W and $d_{Ge} = 180$ μm. In the simulations, the laser emission wavelength, the emission bandwidth and the laser spot radius (r_{sp}) are 1567 nm, 10 nm, and 80 cm, respectively. The local yellow, orange, red or purple color shown here in the two drawings signifies the local temperature of the Ge NP "plate" as is specified by the Kelvin-versus-color scale given here.
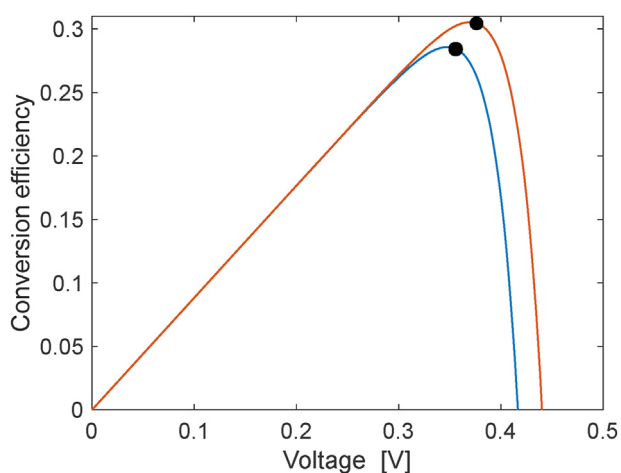

Fig. 2 | Calculated OE conversion efficiency as a function of the Ge PV voltage, for input Er laser power values of 4000 W and 10,000 W and $d_{Ge} = 180$ μm, respectively. In the simulations, the laser emission wavelength and the laser spot radius (r_{sp}) are 1567 nm and 80 cm, respectively. The operative temperature is forced at 300 K.
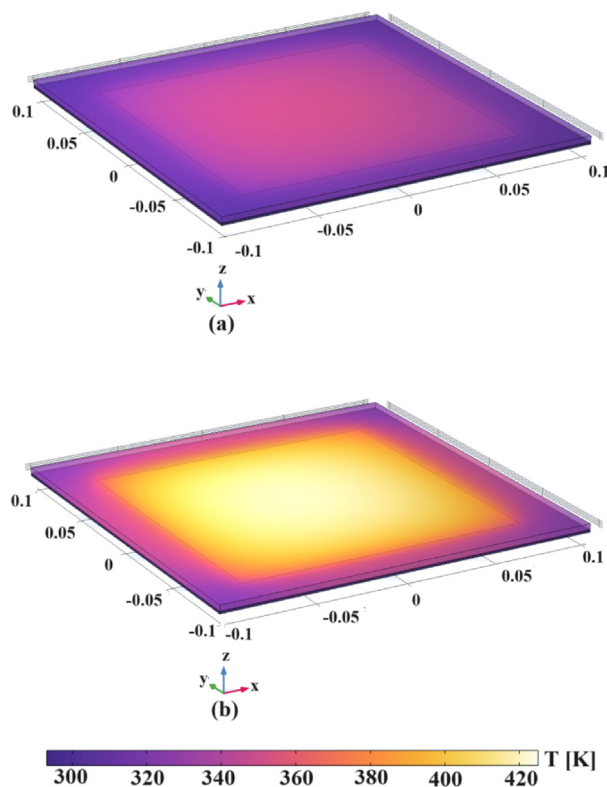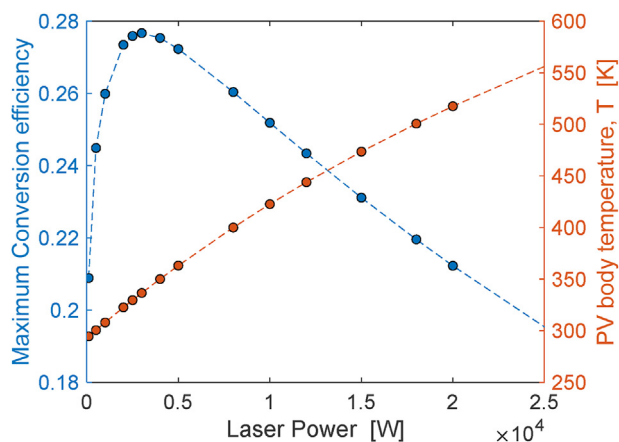
Fig. 4 | Maximum conversion efficiency and Ge PV body temperature as a function of the incoming CW Er laser power ranging from 100 W to 25,000 W and for $d_{Ge} = 180$ µm. In the simulations, the laser emission wavelength, the emission bandwidth and the laser spot radius (r_{sp}) are 1567 nm, 10 nm and 80 cm, respectively.

temperature rises up from 293 K towards 550 K, two opposite trends are recorded. On the one hand, the increase in laser power would lead to an efficiency decrease, while on the other hand, the increase produces an increase in the temperature that in turn increases the Ge absorption coefficient (and then the PV-generated density current) because of the Ge bandgap narrowing. Moreover, our investigations indicate that T_{peak} tends to decrease with decreasing laser emission wavelength (T_{peak} is lower than 293 K for $\lambda < 920$ nm). In this context, the laser heating process will induce a reduction of the maximum conversion efficiency as the PV body temperature increases above 293 K, which is similar to what happens to the PV during sun illumination[30].

Fig. 5 is the principal result of this paper, showing high 1055 to 2412 W/m² electric output densities over the EFL incident-beam 4000 to 10,000 W range mentioned above, operating with 350 K to 423 K PV body temperatures.
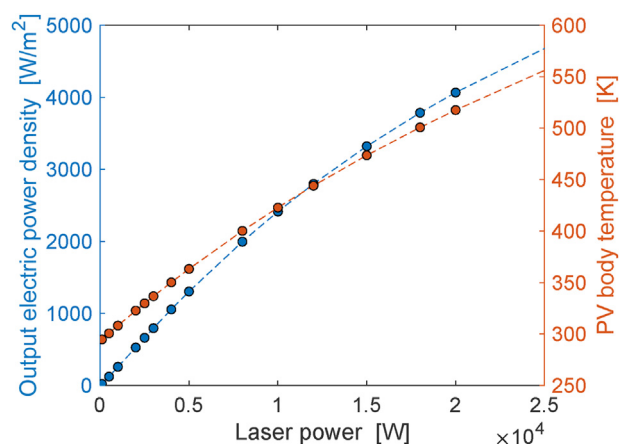

Fig. 5 | Output electrical power density of Ge PV cell and its associated PV body temperature as a function of the EFL CW input-to-PV power, ranging from 100 W to 25,000 W and for $d_{Ge} = 180$ µm. In the simulations, the laser emission wavelength, the emission bandwidth and the laser spot radius (r_{sp}) are 1567 nm, 10 nm and 80 cm, respectively.

The laser power cited in Fig. 4 and 5 is the power that impinges upon the top (front) surface of the PV module. If the beam from the laser transmitter travels a "long distance" through the earth's atmosphere to reach the PV receiver, the effect of the atmosphere upon power transfer[31] can be quantified by turning to Fig. 1 of ref.[16], where the transmittance of the 1.567 µm EFL is shown as 77% radiative transfer across one nautical mile-of-travel at sea level. If we choose, for example, to locate the beam harvester two miles away from the laser source, then the power reaching the PV receiver becomes 59% of the source output.

We discussed earlier the additional YFL conversion offered by Ge PV, and here that performance have been quantified so as to supplement the EFL results. Our numerical modeling of this Ge+YFL OE is presented here in Table 2 along with Ge+EFL. Since the YFL beam conversion was investigated in ref.[16], where Si PV was the receiver, we decided to add several Si+YFL results in this same Table 2 so as to provide a comparison with the Ge+YFL predictions. To make this a fair comparison, we impose the constraint in Table 2 that the Si PV cells must have the same 180 µm thickness as the Ge PV cells. However, the Table does not reveal the full or optimum Si+YFL performances because much higher output power densities were found[16] when increasing the Si cell thickness t from 180 to 500 µm.

YFL's are already available at extremely high CW output power. On the idea that the EFL might someday be extended to 20,000 W, we also decided to determine the 20,000 W CW EFL responses of Ge PV along with the 20,000 W CW Ge+YFL behavior. All of this is summarized in this presentation of efficiency, cell temperature, output power density and output electric power.

An examination of this table shows that Ge offers unique and practical, high-performance EFL conversion. As to YFL conversion, the Ge performances are "mixed", which means that the Ge+YFL efficiencies are lower than those for Ge+EFL, but are still useful and valuable. However, it is also clear that silicon generally "dominates" in the YFL-conversion category.

If we ask about factors that contribute to the predicted lower Ge+YFL conversion, it is noted that the reflectivity of the top glass surface in Fig. 1 is lower at the 1567-nm EFL wavelength than at the 1075-nm YFL wavelength. This means that the Ge+YFL heat source is somewhat higher in the above Flux equation, and that reduces the efficiency.

Results in Table 2 pertain to an individual PV module, in which we took into account of the external radiative efficiency (ERE), a parameter that accounts for carrier recombination losses. Resistive losses were not included. However, the resistance effect in a single "solar type" PV cell does reduce the fill factor FF, which then reduces the efficiency of the cell by dissipating power in the resistance. In particular, the most common parasitic resistances are the series resistance and the shunt resistance. In our PV modules, typical values for area-normalized series and shunt resistances are around 0.5 Ωcm² and in the MΩcm² range, respectively. In this context, due to the large area used for one cell (0.0243 m²), the dominant resistive effect is determined by the series resistance R_{SER}. To accurately represent our case, we shall make the assumptions $d_{Ge} = 180$ µm, laser power of 4000 W and PV body temperature of 350 K. As evidenced in ref.[32], the series and shunt resistances for a Ge PV cell decrease with increasing incident power density. In the thermophotovoltaic approach proposed in ref.[32], the authors measured the series and shunt resistance, respectively, which are 0.02 Ωcm² and 0.22 kΩcm² during spectral irradiance at 2000 K blackbody temperature. Since in our case the operative input power ranges from 4000 W (0.40 W/cm²) to 10,000 W (0.99 W/cm²), and according to Table 2 of ref.[32], it is valid to assume that the series and shunt resistance change from 0.31 to

Soref, R., De Leonardis, F., Moutanabbir, O. & Daligou, G. *Chip* **3**, 100099 (2024)

0.11 Ωcm^2 and from 1.55 to 0.80 $k\Omega cm^2$, respectively. For that reason, the electric power loss is estimated at around 37% for the single PV cell.

MULTI-MODULE GE PV PANEL

If a planar panel is now constructed from an array of cells, and the panel is assumed to be illuminated by the same cylindrical collinated EFL beam with an effective area of 1.00 m^2 and an effective spot radius of 0.564 m that is used for an individual PV module with an area of 0.0243 m^2, then the area of the panel will enter the estimate of its electrical output power, and the output is proportional to the panel area. We now propose that the 32-module array illustrated in Fig. 6 is an optimum choice because of its beam-filling geometry and its 0.78 m^2 area. One approach to determine the panel's output is to simply multiply the Table 2 module outputs by the area-increase-factor of 32; but to be conservative, we shall instead use 80% of the "area factor" because the infrared intensity is distributed nonuniformly across the 1 m^2 beam "spot". Thus 80% of 32 is 25.6 and that is the factor used here to find the panel outputs, which are 666 W (at 350 K panel) and 1510 W (at 423 K panel) for 4000 W and 10,000 W beams, respectively. An important aspect of the panel is the electrical interconnection of cells that is chosen. As we discussed in ref.[16], it is essential to connect the 32 modules in series, and when that is done, the series resistance of each cell induces only a negligible electric power loss in the panel.

It should be noted that Fig. 6 has immediate application to thermophotovoltaic TPV sensing. For example[32], it has quantified OE conversion of 9.7% to 11.8% OE for the 2000 K filtered blackbody radiation intensity of 3.66 to 36.6 W/cm^2 incident upon the Ge TPV NP diode. For our 0.78 m^2 Ge TPV panel, this TPV result translates immediately to a DC electric output of 2769 W to 33,687 W from the panel in Fig. 6.

Moreover, there are potential alternative semiconductor materials (alternatives to Germanium) that could be utilized to construct the EFL-harvesting PV panel. However, those PV- material choices have some

disadvantages. To be specific, the compound semiconductor GaSb has $E_g = 0.68$ eV at 300 K, while InN has $E_g = 0.65$ eV at 300 K, and both of these PV materials could efficiently convert the 1567-nm EFL, but there are issues of GaSb/InN wafer-size availability and wafer cost. In principle, the PV panel could be constructed from InGaAs or InGaAsP alloy whose alloy composition would be chosen to give absorption α at 300 K of 50 to 100 cm^{-1} at the EFL wavelength, according to the $t \sim 1/\alpha$ design rule. In that case, the 100-to-200-μm PV layers required would present very severe epitaxy challenges for the alloys. Regarding the narrow-bandgap semiconductors InAs, InSb, PbSe, and PbS (all of whose room-temperature α is "high" at 1567 nm), these materials are probably not viable to be used for the PV panel. This is ascribed to the fact that the $1/\alpha$ approach gives a sub-micron PV NP layer, which implies that the panel will heat up to an unmanageably high temperature during UHP illumination.

Returning to the Ge panel, it should be mentioned that there is the possibility of attaining high-speed optical communications[33,34] simultaneously in conjunction with the DC energy harvesting; a dual DC+RF function of the system, operating along the lines proposed in ref.[35]. In the present case, a small-area RF electro-optical modulator (external to the CW laser) would be placed within the laser's two-lens collimating optics to intercept the beam in a focal region where the beam diameter is relatively small. That modulator[36,37] would put RF information on the beam with a small depth-of-modulation, and then at the remote receiver, a small-area RF photodetector would be placed at the rear face of the large PV panel to "sample" the small amount of the infrared beam that is transmitted through the PV panel (the "residual transmission" of the panel), and that photodetector[38,39] would demodulate the intensity-variations, giving the signals that were put onto the laser beam. Both RF devices could use Ge or SiGe as their active material[40].

CONCLUSIONS

In the current work, we have proposed and analyzed an efficient, directed-beam, electric-energy harvesting system which is comprised of the 1567-nm UHP CW Er-doped fiber laser source and the monocrystal Germanium 32-PN-diode-module series-connected photovoltaic "panel" receiver sited a long distance away from the collimated and directed laser. The theoretical modeling results are favorable because 666 W to 1512 W of electric power generation is predicted for 4 kW to 10 kW incident beaming, with the passively heat-sinked panel rising to 350 to 423 K during operation. An added benefit is that the same Ge panel gives 435 W to 947 W electric harvesting of the 1075-nm Yb-doped 4 kW to 10 kW fiber lasers.

REFERENCES

1. Algora, C. et al. Beaming power: photovoltaic laser power converters for power-by-light. *Joule* **6**, 340−368 (2022). https://doi.org/10.1016/j.joule.2021.11.014.
2. Gou, Y. et al. High-performance laser power converters with resistance to thermal annealing. *Opt. Express* **32**, 8335−8342 (2024). https://doi.org/10.1364/OE.515130.
3. Liu, H., Zhang, Y., Hu, Y., Tse, Z. & Wu, J. Laser-power transmission and its application in laser-powered electrical motor drive. *Power Electron. Drives* **6**, 167−184 (2021). https://doi.org/10.2478/pead-2021-0010.
4. Haas, H., Elmirghani, J. & White, I. Optical wireless communication. *Phil. Trans. R. Soc. A.* **378**, 20200051 (2020). https://doi.org/10.1098/rsta.2020.0051.
5. Javed, N., Nguyen, N.-L., Naqvi, S. F. A. & Ha, J. Long-range wireless optical power transfer system using an EDFA. *Opt. Express* **30**, 33767−33779 (2022). https://doi.org/10.1364/OE.468766.
6. Zheng, Y. et al. Wireless laser power transmission: recent progress and future challenges. *Space Sol. Power Wire. Trans.* **1**, 17−26 (2024). https://doi.org/10.1016/j.sspwt.2023.12.001.
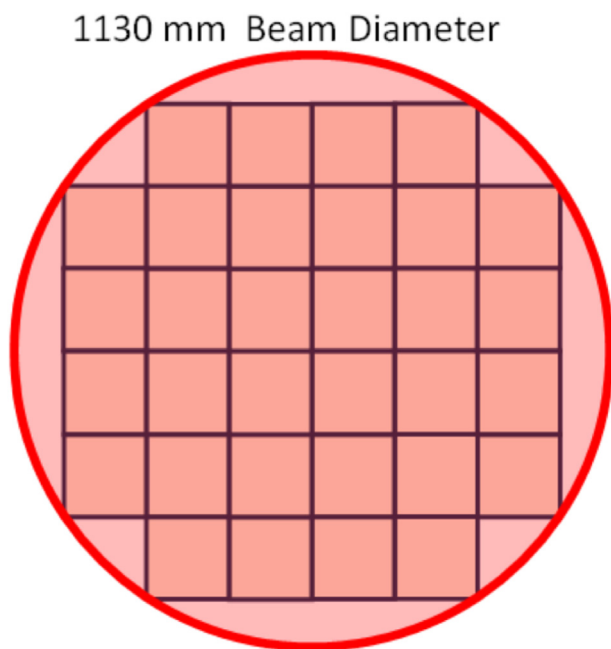
1130 mm Beam Diameter

Fig. 6 | Proposed Ge PV panel comprised of 32 identical interconnected PV modules in a layout offering strong overlap with the 1567-nm collimated beam.

7. Jin, K. & Zhou, W. Wireless laser power transmission: a review of recent progress. *IEEE Trans. Power Electron.* **34**, 3842−3859 (2019). https://doi.org/10.1109/TPEL.2018.2853156.

8. Xu, W., Wang, X., Li, W., Li, S. & Lu, C. Research on test and evaluation method of laser wireless power transmission system. *Eurasip J. Adv. Signal Process.* **2022**, 20 (2022). https://doi.org/10.1186/s13634-022-00852-9.

9. Mohammadnia, A., Ziapour, B. M., Ghaebi, H. & Khooban, M. H. Feasibility assessment of next-generation drones powering by laser-based wireless power transfer. *Opt. Laser Technol.* **143**, 107283 (2021). https://doi.org/10.1016/j.optlastec.2021.107283.

10. He, T. et al. Analysis and experiment of laser energy distribution of laser wireless power transmission based on a powersphere receiver. *Photonics* **10**, 844 (2023). https://doi.org/10.3390/photonics10070844.

11. Zhou, W. & Jin, K. Power control method for improving efficiency of laser-based wireless power transmission system. *IET Power Electron.* **13**, 2096−2105 (2020). https://doi.org/10.1049/iet-pel.2019.1372.

12. Eom, J., Kim, G. & Park, Y. Maximizing wireless power transfer for electric vehicles with high-intensity laser power beaming and optical orthogonal frequency division multiplexing. *Transport. Res. Proceed.* **70**, 123−129 (2023). https://doi.org/10.1016/j.trpro.2023.11.010.

13. Yao, D. et al. Laser wireless power transfer and thermal regulation method driven by transient laser grating. *AIP Adv.* **12**, 105001 (2022). https://doi.org/10.1063/5.0106968.

14. Jin, K. & Zhou, W. Wireless laser power transmission: review of recent progress. *IEEE Trans. Power Electron.* **34**, 3842−3859 (2019). https://doi.org/10.1109/TPEL.2018.2853156.

15. Zhang, Q. et al. Distributed laser charging: a wireless power transfer approach. *IEEE Internet Things J.* **5**, 3853−3864 (2018). https://doi.org/10.1109/JIOT.2018.2851070.

16. Soref, R., De Leonardis, F., Daligou, G. & Montanabbir, O. Directed high-energy infrared laser beams for photovoltaic generation of electric power at remote locations. *APL Energy* **2**, 026101 (2024). https://doi.org/10.1063/5.0197277.

17. Osterthun, N., Neugebohrn, N., Gehrke, K., Vehse, M. & Agert, C. Spectral engineering of ultrathin germanium solar cells for combined photovoltaic and photosynthesis. *Opt. Express* **29**, 938−950 (2021). https://doi.org/10.1364/OE.412101.

18. Lombardero, I., Ochoa, M., Miyashita, N., Okada, Y. & Algora, C. Theoretical and experimental assessment of thinned germanium substrates for III−V multijunction solar cells. *Prog. Photovolt.* **28**, 1097−1106 (2020). https://doi.org/10.1002/pip.3281.

19. Hekmatshoar, B., Shahrjerdi, D., Hopstaken, M., Fogel, K. & Sadana, D. K. High-efficiency heterojunction solar cells on crystalline germanium substrates. *Appl. Phys. Lett.* **101**, 032102 (2012). https://doi.org/10.1063/1.4737166.

20. Fernandez, J., Janz, S., Suwito, D., Oliva, E. & Dimroth, F. Advanced concepts for high-efficiency germanium photovoltaic cells. In *2008 33rd IEEE Photovoltaic Specialists Conference*, 1−4 (IEEEE, 2008). https://doi.org/10.1109/PVSC.2008.4922631.

21. Sun, G., Chang, F. & Soref, R. A. High efficiency thin-film crystalline Si/Ge tandem solar cell. *Opt. Express* **18**, 3746−3753 (2010). https://doi.org/10.1364/OE.18.003746.

22. Azizman, M. S. A. et al. Mixed cations tin-germanium perovskite: a promising approach for enhanced solar cell applications. *Heliyon* **10**, e29676 (2024). https://doi.org/10.1016/j.heliyon.2024.e29676.

23. Zhu, X. et al. Evaluation of electricity generation on GeSn single-junction solar cell. *Int. J. Energy Res.* **46**, 14526−14533 (2022). https://doi.org/10.1002/er.8111.

24. Zhou, Z., Liu, W., Guo, Y., Huang, H. & Ding, X. Design simulation and optimization of germanium-based solar cells with micro-nano cross-cone absorption structure. *Coatings* **12**, 1653 (2022). https://doi.org/10.3390/coatings12111653.

25. CW Laser Series ELS-4000. IPG Photonics. https://www.ipgphotonics.com/products/lasers/industrial-cw-fiber-lasers/erbium-thulium-raman-fiber-lasers.

26. Ge-Germanium. Ioffe Institute. https://www.ioffe.ru/SVA/NSM/Semicond/Ge/.

27. Tran, H. et al. Systematic study of $Ge_{1-x}Sn_x$ absorption coefficient and refractive index for the device applications of Si-based optoelectronics. *J. Appl. Phys.* **119**, 103106 (2016). https://doi.org/10.1063/1.4943652.

28. Chang, G.-E., Yu, S.-Q. & Sun, G. "GeSn rule-23"-the performance limit of GeSn infrared photodiodes. *Sensors* **23**, 7386 (2023). https://doi.org/10.3390/s23177386.

29. Baran, V. et al. A comprehensive study on a stand-alone germanium (Ge) solar cell. *J. Electron. Mater.* **49**, 1249−1256 (2020). https://doi.org/10.1007/s11664-019-07712-7.

30. Singh, P. & Ravinda, N. Temperature dependence of solar cell performance—an analysis. *Sol. Energy Mater. Sol. Cells* **101**, 36−45 (2012). https://doi.org/10.1016/j.solmat.2012.02.019.

31. Fahey, T., Islam, M., Gardi, A. & Sabatini, R. Laser beam atmospheric propagation modelling for aerospace LIDAR applications. *Atmosphere* **12**, 918 (2021). https://doi.org/10.3390/atmos12070918.

32. Gamel, M. M. A. et al. Performance of Ge and $In_{0.53}Ga_{0.47}As$ thermophotovoltaic cells under different spectral irradiances. *IEEE Access* **9**, 37091−37102 (2021). https://doi.org/10.1109/ACCESS.2021.3062075.

33. Garg, D. & Nain, A. Next-generation optical wireless communication; a comprehensive review. *J. Opt. Commun.* **44**, s1535−s1550 (2023). https://doi.org/10.1515/joc-2020-0254.

34. Walsh, S. M. et al. Demonstration of 100 Gbps coherent free-space optical communications at LEO tracking rates. *Sci. Rep.* **12**, 18345 (2022). https://doi.org/10.1038/s41598-022-22027-0.

35. Kessler-Lewis, E., Polly, S. J., Sacchitella, E., Hubbard, S. M. & Hoheisel, R. Demonstration of a monolithically integrated hybrid device for simultaneous power generation and data modulation. *IEEE J. Photovoltaics* **14**, 272−280 (2024). https://doi.org/10.1109/JPHOTOV.2024.3359448.

36. Soref, R. A., Sun, G. & Cheng, H. H. Franz-Keldysh electro-absorption modulation in germanium-tin alloys. *J. Appl. Phys.* **111**, 123113 (2012). https://doi.org/10.1063/1.4730404.

37. Bennett, B. R. & Soref, R. A. Analysis of franz-keldysh electro-optic modulation in InP, GaAs, GaSb, InAs, and InSb. In *1987 Conference on Optoelectronic Materials, Devices, Packaging, and Interconnects*, 158−168 (SPIE, 1987). https://doi.org/10.1117/12.967524.

38. Lischke, S. et al. Ultra-fast germanium photodiode with 3-dB bandwidth of 265 GHz. *Nat. Photonics* **15**, 925−931 (2021). https://doi.org/10.1038/s41566-021-00893-w.

39. Li, D. et al. High-speed and high-power Ge-on-Si photodetector with bilateral mode-evolution-based coupler. *Photonics* **10**, 142 (2023). https://doi.org/10.3390/photonics10020142.

40. Moontragoon, P., Soref, R. A. & Ikonic, Z. The direct and indirect bandgaps of unstrained $Si_xGe_{1-x-y}Sn_y$ and their photonic device applications. *J. Appl. Phys.* **112**, 073106 (2012). https://doi.org/10.1063/1.4757414.

MISCELLANEA

Author contributions **Richard Soref:** Conceptualization, Supervision, Writing – original draft, Writing – review & editing. **Francesco De Leonardis:** Conceptualization, Formal analysis, Software, Writing – review & editing. **Oussama Moutanabbir:** Validation, Writing – review & editing. **Gerard Daligou:** Validation, Writing – review & editing.

Declaration of Competing Interest The authors declare no competing interests.